Nanotechnology and Nano-Interface Controlled Electronic Devices
Editors: M. Iwamoto, K. Kaneto and S. Mashiko

CHAPTER 8

Materials and devices for ultrafast molecular photonics

Toshihiko Nagamura

Molecular Photonics Laboratory, Research Institute of Electronics, Shizuoka University, 3-5-1 Johoku, Hamamatsu 432-8011, Japan
E-mail: nagamura@rie.shizuoka.ac.jp

1. Introduction

Novel materials, devices and systems are required for much faster data processing, much higher recording density, or much more specific and efficient sensing. Ultrafast switching materials which work in less than 1 ps are essential for teraHerz (THz) optical communication. Several attempts have been made for this purpose, which include optical switching by tunneling bi-quantum well semiconductors or organic nonlinear optical materials [1]. Magnetic “hard” disks and heat-mode optical disks such as phase change

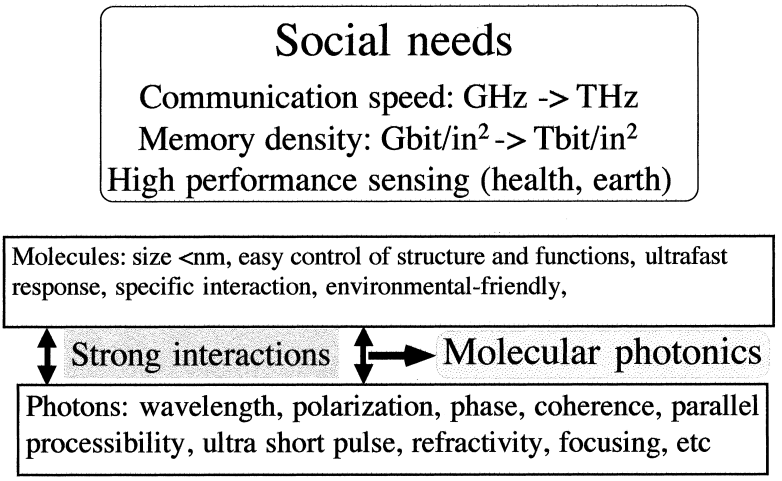

Fig. 1: Why and how molecular photonics?

or magneto-optical memories have rapidly been increasing their recording density owing to the development of new pick-up heads or blue semiconductor lasers. But there is a physical limit in such conventional memories recording data bit by bit in a serial way on the surface or in the thin surface layer of recording materials.

Organic molecules have many useful optical and electronic functions that can be easily controlled by the structures, substituents, or external fields. Specific interactions or organization of molecules further can afford much higher functions than isolated or randomly distributed molecules. Photons have many superior properties such as wavelength, polarization, phase, ultrashort pulse, or parallel processibility. Through strong interactions of molecules or molecular assemblies with photons, many superior properties of photons can be directly converted to changes in physical properties of materials such as fluorescence, absorption, refractive index, conductivity, or optical nonlinearity. These interactions will be utilized as molecular photonics with ultra high speed, ultra high density or high performance sensing as schematically shown in Fig. 1. Excited state formation, photochromism, photoinduced electron transfer are some examples among them. Photon-mode recording or switching based on these changes of electronic states can therefore achieve ultrafast multiple or three-dimensional recording and parallel processing with ultimate spatial resolution at a molecular level. There will be no doubt that molecular photonics based on interactions of molecules and photons has many advantages as compared with electric or photoelectric switching, heat-mode or magnetic recording, switching based on liquid crystals or thermal phenomena.

We have been making efforts to develop new molecular photonics materials and devices by making various organized molecular systems and by optically controlling their electronic states. So far we have achieved photoinduced electrochromism, which is color changes due only to the photoinduced electron transfer and reverse reactions, molecular control of the lifetime and the wavelength of colored species over extremely wide ranges, amplified fluorescence quenching in LB films, photon-mode super-resolution

to exceed the diffraction limit of light in optical memory based on transitory photobleaching of phthalocyanine derivatives, ultrafast all-optical two-dimensional control of reflectance and parallel optical self-holding switch based on photoinduced complex refractive index changes [2,3]. In the present chapter, some of our recent achievements will be discussed on materials and devices for ultrafast molecular photonics.

2. Materials and methods for ultrafast photoresponse measurements

The structures of typical compounds employed in our study are shown in Fig. 2. 1,2-Dimethoxyethane (DME) and methanol solutions of $TFPB^-$ or iodide (I^-) salts of polymeric 4,4′-bipyridinium (PV^{2+}) were used together with polymer films cast or spin-coated from these solutions. The content of 4,4′-bipyridinium ions in a PV^{2+} polymer is 3.3×10^{-4} mol/g. Various types styrylpyridinium (NS^+, DCS^+, NS^+CnNS^+) tetraphenylborate (TPB^-) salts in DME were also employed to study ultrafast absorption changes in the visible and near-infrared (NIR) region. Several derivatives of phthalocyanines including water soluble copper-phthalocyanine (CuPcS) and zinc-phthalocyanine (ZnPcS) were used for photon-mode spatial light modulation. Phthalocyanines were used in solutions or in poly(vinyl alcohol) (PVA) films. A photochromic spiropyran derivative, 1,3,3-trimethylindolino-6′-nitrobenzopyrylospiran (SP) was dispersed in polystyrene or Arton® (JSR Co. Ltd.), which became a colored photomerocyanine (PM) type upon UV irradiation.

For ultrafast dynamics studies, these dyes were excited in air at room temperature by the second harmonics (400 nm) of a femtosecond (fs) Ti : sapphire laser with a regenerative Ti : sapphire amplifier and a double path amplifier pumped with the second harmonics (532 nm) of a Nd : YAG laser. The amplified Ti : sapphire laser delivered pulses with a FWHM of 200–250 fs, 10 Hz repetition, a maximum power of 6 mJ/pulse at 800 nm. The fs probe white light was obtained by focusing the residual 800 nm light into a cell containing D_2O/H_2O (2 : 1) mixture after passing through a BBO crystal to obtain the second harmonics. The transient absorption and the dynamics were observed with a Photonic Multi-channel Analyzer (PMA; Hamamatsu Photonics) system using a dual photodiode array (Hamamatsu Photonics C6140) for the UV–visible and an InGaAs multichannel detector (Hamamatsu Photonics C5890-256) for the NIR absorption using an optical delay system. The intensities of the probe light with and without the pump pulses were averaged by 20 times. The block diagram of the fs transient absorption measurement system is shown in Fig. 3.

For measuring basic properties of reflection type spatial light modulation or parallel optical switching, the sample plate was index-matched with a BK7 prism, which was set on a computer-controlled rotating stage. The writing beam was a ns OPO laser at 670 nm or the third harmonic (355 nm) of Nd : YAG laser; each with 8 ns pulse width, 0.03–2 mJ/pulse, and ca. 0.2 cm^2 beam area. He–Ne laser (543.5 nm) through a half-wave plate, a polarizer, and a chopper was used as a reading beam. The time dependence of a reflected intensity at a given incident angle upon ns laser excitation at different powers was detected with a photomultiplier and was recorded with a digital oscilloscope terminated with 50 ohm. The spatial resolution was evaluated by using a

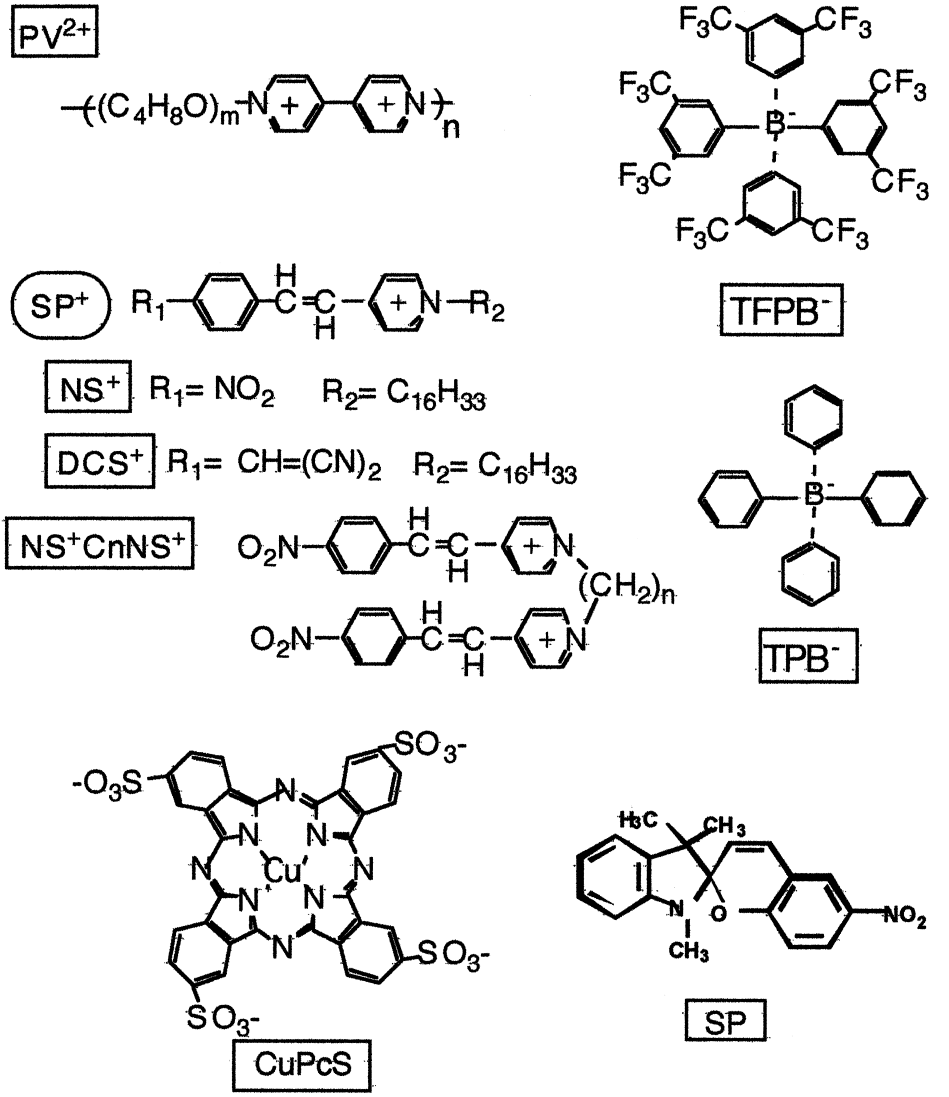

Fig. 2: The structures and abbreviations of typical compounds employed.

USAF Test Target as a mask. In order to measure reflectance changes of fs white light as a reading light upon excitation by 400 nm fs pulses as a writing light, an Arton® film with spiropyran spin-coated on silver film was set with a prism on a rotating stage as schematically shown in Fig. 4.

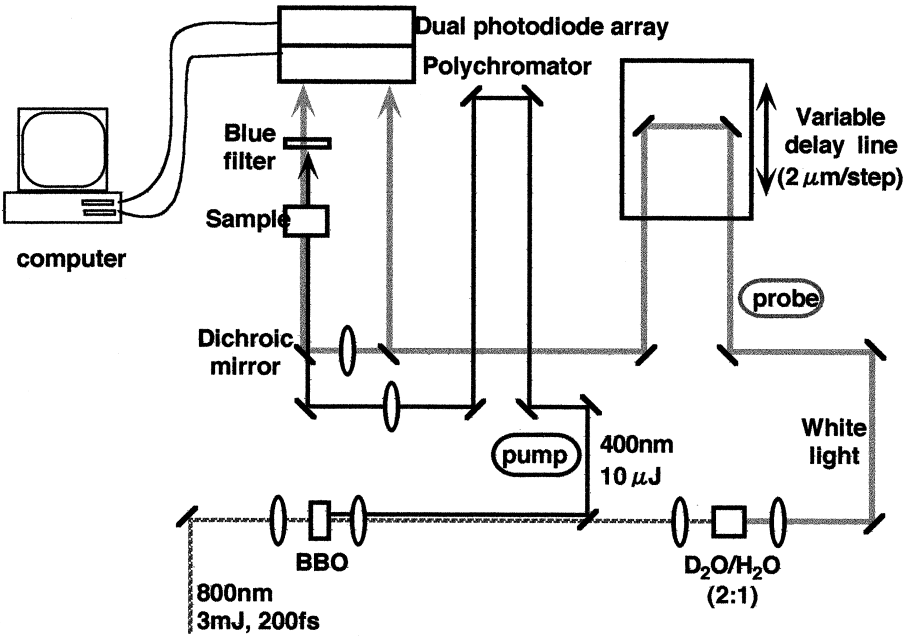

Fig. 3: The block diagram of a fs laser flash photolysis system.

3. Absorption changes over wide ranges of wavelength and time by photoinduced electrochromism of ion-pair charge-transfer complexes

3.1. Photoinduced electrochromism in 4,4′-bipyridinium salts with various counter ions

Various photochromic systems employing polymeric thin films or Langmuir–Blodgett (LB) films have recently attracted much interest in view of their promising applicability to high-speed and high-density photon-mode optical memory [2–7]. The photochromism reported so far involves changes of chemical bonds such as heterolytic cleavage of a pyran ring in spiropyrans, ring opening and closing in diarylethenes and fulgides, or *trans–cis* isomerization in azobenzenes [4–7]. Recently we have reported novel photoinduced electrochromism as schematically shown in Fig. 5 [2,3,8–24]. It is the color change due to photoinduced electron transfer in ion-pair charge transfer (IPCT) complexes of 4,4′-bipyridinium salts with tetrakis[3,5-bis(trifluoromethyl)phenyl]borate [25] (abbreviated to $TFPB^-$) and thermal back electron transfer reactions. No changes of chemical structure were involved in photochromism. $TFPB^-$ and iodide (I^-) salts of 4,4′-bipyridinium ions showed pale yellow and red colors, respectively, though each ion is colorless. These new absorption spectra above 350 nm in solutions were attributed to the IPCT complexes with 4,4′-bipyridinium ion as an acceptor and $TFPB^-$ or I^- as a donor. It was thus demonstrated that these ion pairs made electronic interactions at the ground state partially transferring electronic charges from a donor to an acceptor. No

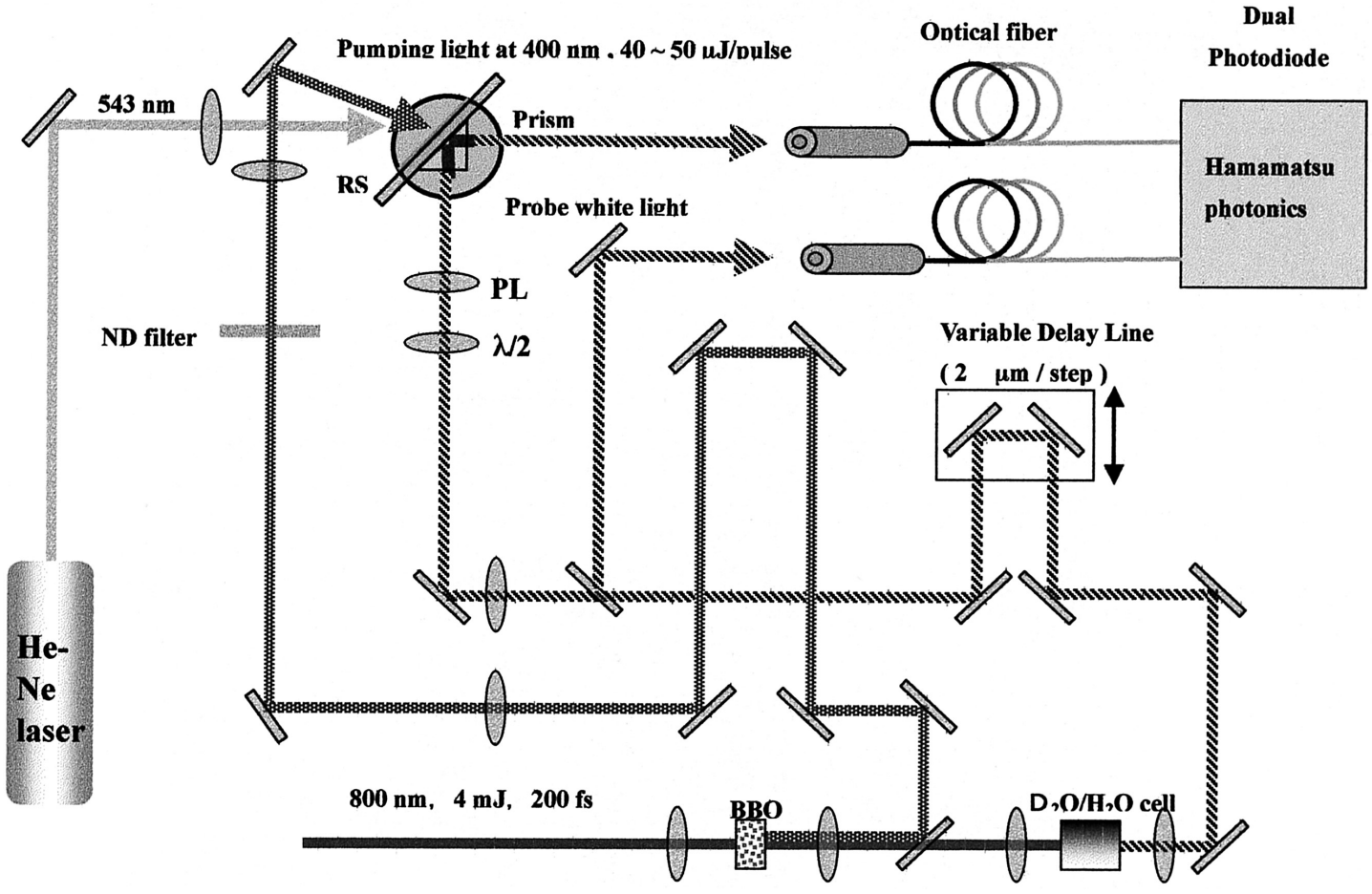

Fig. 4: Schematic representation of measurement systems for the incident angle and the time dependences of reflected intensity in guided mode thin films by fs laser.

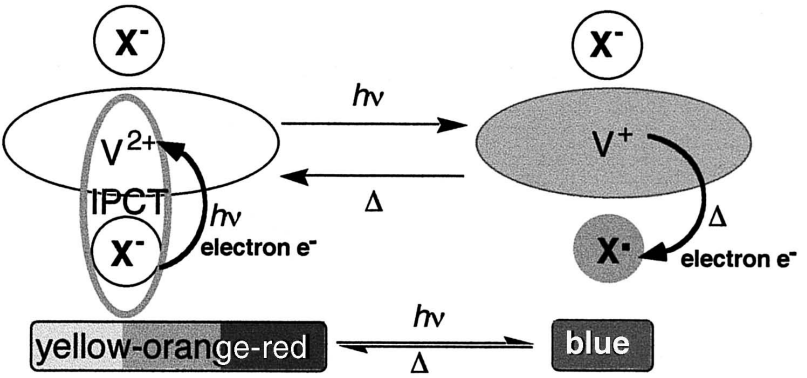

Fig. 5: Schematic representation of photoinduced electrochromism in 4,4′-bipyridinium IPCT salts.

color changes were observed with I^- salts by steady photolysis, which is in contrast to $TFPB^-$ salts.

From steady and laser photolysis results it has been shown that 4,4′-bipyridinium radical cations, which escaped from the geminate reaction immediately after the photoinduced electron transfer in less than 1 ps [22] upon IPCT excitation, became metastable owing to the bulk and chemical stability of $TFPB^-$, to the restriction of molecular motion by the microenvironment, and also probably to the very high exothermicity of the reverse reaction in the Marcus inverted region [26,27]. Highly sensitive detection of photoinduced electrochromism and transient absorption spectra in ultra-thin LB and polymer films have been achieved by the conventional and the white-light optical waveguide method [28–33]. Such photoinduced electrochromism may be applied to ultrafast photon-mode optical memory and to redox sensors.

3.2. Ultrafast dynamics of photoinduced electrochromism

Immediately upon excitation of an IPCT band with a fs laser at 400 nm, transient absorption was observed for both salts in solutions with a peak at about 600 nm, characteristic of 4,4′-bipyridinium radical cations. Fig. 6 shows the transient absorption spectra of $PV^{2+}(I^-)_2$ in methanol solution. A marked increase in the absorbance of the 4,4′-bipyridinium radical cations took place with a rise time of about 0.3 ps upon excitation. 4,4′-Bipyridinium radical cations were thus formed in a fs time scale by the photoinduced electron transfer from a donor I^- to an acceptor 4,4′-bipyridinium upon IPCT excitation [22]. The time profiles of transient absorption at 600 nm are shown in Fig. 7 for (a) $PV^{2+}(I^-)_2$ in a film cast from DME and (b) $PV^{2+}(TFPB^-)_2$ in DME solutions. Both of them showed a very rapid rise in about 0.3 ps, which was almost the same as the time resolution of our fs Ti : sapphire laser measurement system with a regenerative amplifier. Similar extremely rapid formation of 4,4′-bipyridinium radical cations was observed for $PV^{2+}(I^-)_2$ salts in methanol and dimethylsulfoxide solutions upon IPCT excitation, respectively. These results demonstrated that the charge separated 4,4′-bipyridinium radical cations were formed directly upon IPCT excitation because of

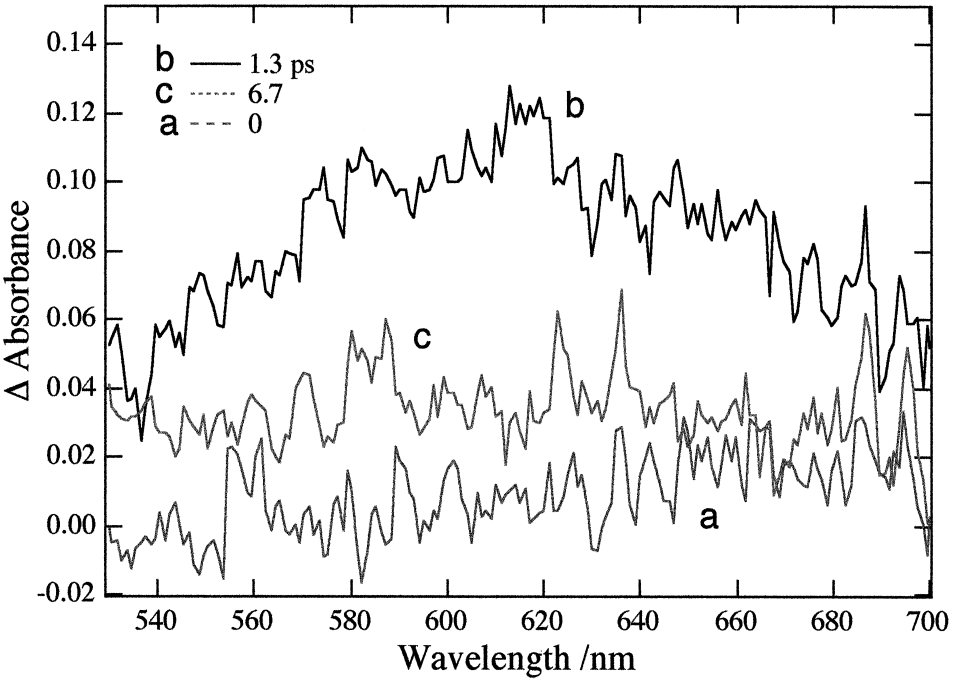

Fig. 6: Transient absorption spectra of $PV^{2+}(I^-)_2$ in methanol solution upon fs laser excitation at 400 nm.

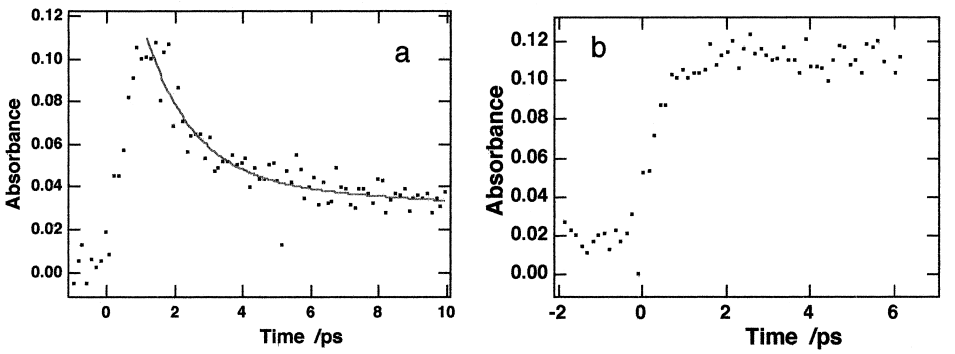

Fig. 7: The time profiles of transient absorption at 600 nm for (a) $PV^{2+}(I^-)_2$ in a film cast from DME and (b) $PV^{2+}(TFPB^-)_2$ in DME solutions.

the nature of IPCT absorption bands that the electrons correlated with the IPCT band are transferred partially at the ground state and completely at the excited state. Such a situation is very different from usual photochromism, which is caused by various changes of chemical bonds mainly via the excited singlet state. No transient absorption was observed for $PV^{2+}(I^-)_2$ in DME solutions, which was most probably due to the

decreased distance between ion pairs in such a less polar solvent and an appropriate thermodynamic driving force ($-\Delta G^0$) for reverse electron transfer reactions [26,27].

The decay behavior due to the reverse electron transfer was found to depend markedly on the microenvironment and the counter anion. The lifetime (τ) and a fraction of a major component for $PV^{2+}(I^-)_2$ was 1.2 ps and 86% in films cast from DME as compared with 4.0 ps and 73% in methanol solutions [22]. Photogenerated 4,4′-bipyridinium radical cations disappeared completely during 10 Hz excitation, which corresponded well with the fact that no steady color changes were observed for $PV^{2+}(I^-)_2$ in solutions and in cast films upon IPCT excitation. No decay was observed on the same time scale, as shown in Fig. 7(b) for $PV^{2+}(TFPB^-)_2$. About a half decayed with $\tau = 71$ ps and the rest survived for an extremely long time corresponding to the reversible and persistent color changes observed by steady photolysis [20]. The lifetimes of photogenerated 4,4′-bipyridinium radical cations were thus controlled over a very broad range from about 1 ps to almost infinity by the $-\Delta G^0$ value, the polarity of solvents and microenvironments in solid films. The present result of color change in about 0.3 ps with IPCT complexes of PV^{2+} is the fastest response reported so far among materials which show steady photochromism. It will help a great deal to develop novel optical memory and also THz all-optical switching devices using visible light.

3.3. Charge resonance band in the near infrared region and its ultrafast dynamics

Recently we have also reported, for the first time, the charge resonance (CR) band due to dimer radical cation formation as a broad absorption with a peak at 950–2000 nm upon steady photoexcitation of styrylpyridinium derivatives such as tetraphenylborate (TPB^-) salts of 1-hexadecyl-4-(4-dicyanovinylstyryl)pyridinium (DCS^+), 1-hexadecyl-4-(4-nitrostyryl)pyridinium (NS^+) or 1,n-bis(4-nitrostyrylpyridinium)alkane (NS^+CnNS^+), as shown in Fig. 2, in solutions at room temperature by steady photolysis [34–46]. The absorption spectra after irradiation (> 365 nm) for TPB^- salts of DCS^+ and NS^+in DME are shown in Fig. 8 with respect to those before irradiation. In addition to the absorption spectra in the visible region due to the radical formation, broad specific absorption spectra were observed in the NIR region. The peak wavelength and shape of the latter spectra depended on the substituents. They were assigned to a CR band as schematically shown in Fig. 9 in a dimer radical cation which was formed between a styrylpyridinium cation and a photogenerated styrylpyridinyl radical. We have also observed the CR band with a peak at 1500–1700 nm as a charge resonance band for intramolecular dimer radical cations, as shown in Fig. 10 for NS^+C3NS^+, NS^+C4NS^+, and NS^+ in acetonitrile [38]. It is clearly shown that two very strong CR bands with peaks at 950 and 1700 nm were observed only in NS^+C3NS^+ due to intramolecular dimer radical cations. The CR band energy is twice the stabilization energy of the dimer radical cations which is controlled by several factors such as the extent of overlap of two chromophores, their mutual distance, and/or the polarity of solvents. The CR bands at 950 and 1700 nm were assigned to fully and partially overlapped dimer radical cations, respectively. Very recently we also reported fairly strong and unusual absorption changes in 800–2200 nm due to the intramolecular CR band of styrylpyridinyl radicals, formed by steady photolysis of newly synthesized *meso*-2,4-bis(4-(4′-nitrostyryl)

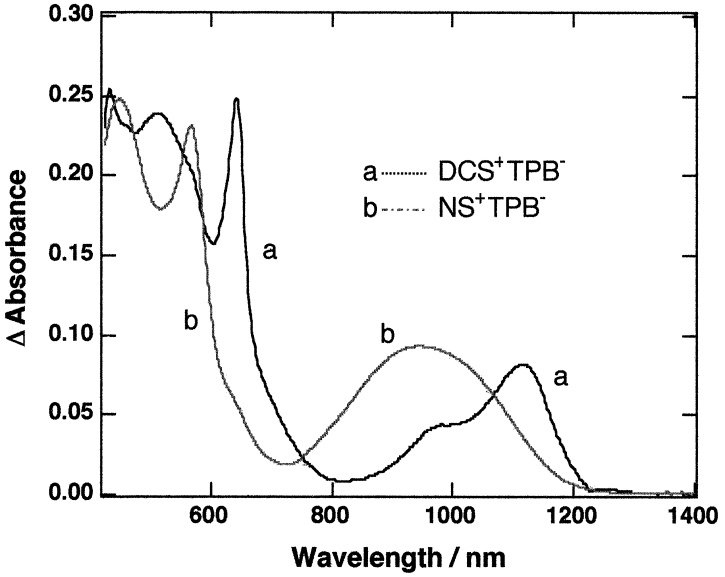

Fig. 8: Difference absorption spectra of (a) $DCS^{+}TPB^{-}$ and (b) $NS^{+}TPB^{-}$ in DME after irradiation at > 365 nm in degassed conditions.

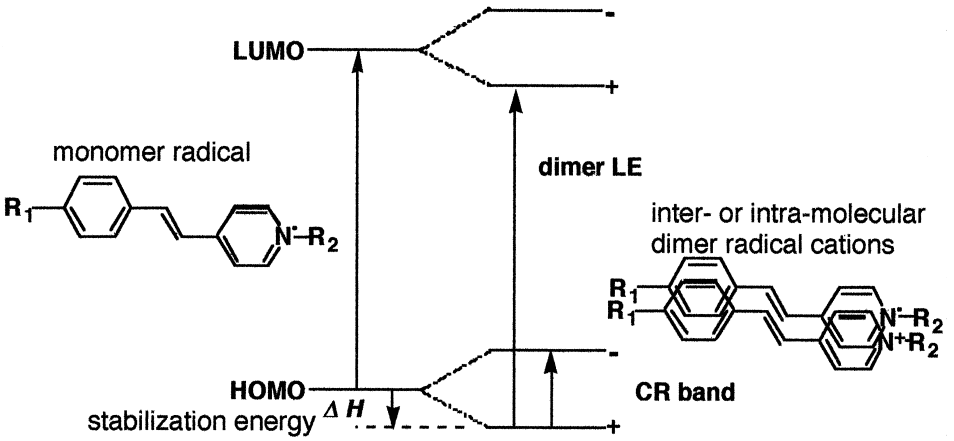

Fig. 9: Schematic representation of energy levels for monomer radical and dimer radical cations, ΔH is the stabilization energy of dimer radical cations.

pyridinium)pentane ditetraphenylborates, during storage in the dark in solutions at room temperature, clearly indicating the change in conformation and overlapping of two chromophores in dimer radical cations which was controlled by the molecular structure [45,46].

As shown in Fig. 11, the rise of absorption spectra at the visible region due to radical formation and at the near-IR region due to the CR band was observed in less than 1

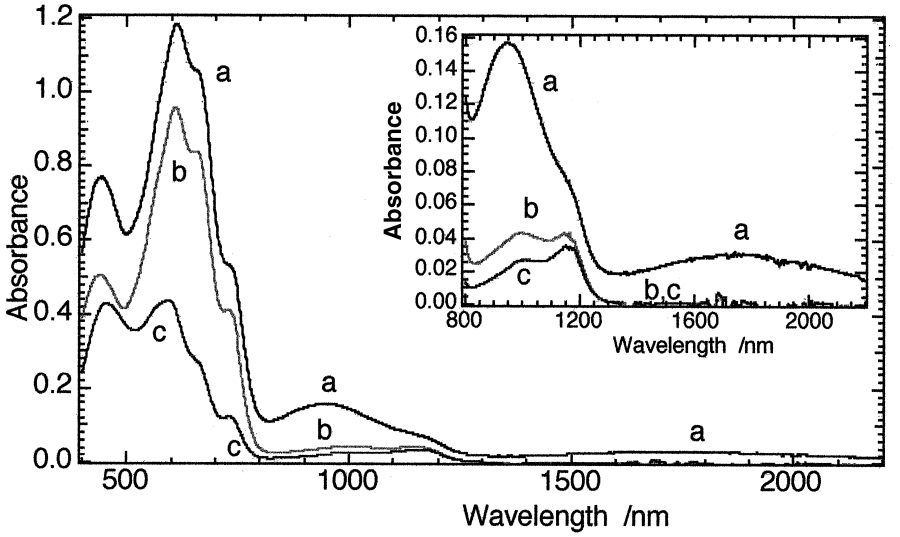

Fig. 10: Absorption spectra for TPB^- salts of (a) NS^+C3NS^+, (b) NS^+C4NS^+, (c) NS^+ irradiated in acetonitrile by a Xe–Hg lamp at $\lambda_{ex} > 365$ nm at room temperature in degassed conditions.

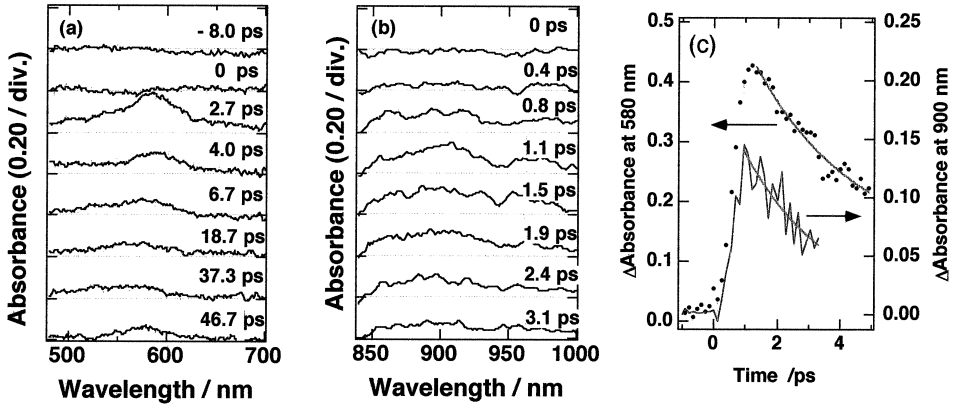

Fig. 11: Transient absorption in (a) the visible and (b) near infrared region together with (c) time dependences at 580 and 900 nm upon fs laser excitation of NS^+TPB^- in DME at room temperature.

ps upon a fs laser excitation at 400 nm. These results indicated that the dimer radical cations were formed immediately after the photoinduced electron transfer reaction. The CR band at 900 nm in NS^+TPB^- decayed single-exponentially ($\tau = 3.3$ ps) [39]. The transient absorption at 580 nm showed double exponential decay with lifetimes of 3.3 and 11.4 ps. Similar results were obtained for DCS^+TPB^-; the decay at 960 nm with $\tau = 3.2$ ps, and that at 650 nm with lifetimes of 3.8 ps for a fast component and 17.4 ps for a slow one [39]. The difference in the decay behavior at the visible and the near-IR region was explained as follows. While the NIR region absorption is attributed to the

dimer radical cation alone as the CR band, both the monomer radical and the dimer radical cation contribute to the absorption in the visible region as a HOMO–LUMO transition as schematically shown in Fig. 9. The fast component in the visible region and that in the NIR absorption gave almost the same lifetime. They were attributed to the reverse electron transfer reactions from the dimer radical cation ($SP^+ \cdots SP^\bullet$) to the $TPB^\bullet$ radical. Then the slow component in the visible region was most probably due to the reverse electron transfer reaction from the monomer radical ($SP^\bullet$) to the $TPB^\bullet$ radical.

The higher rate of the reverse electron transfer in the dimer radical cations than in the monomer radicals was explained by the classical Marcus theory as follows [26,27]. The $-\Delta G^0$ values for the reverse electron transfer from $NS^\bullet$ and $DCS^\bullet$ to $TPB^\bullet$ were estimated as 1.69 and 1.61 eV from the redox potentials, respectively. The reduction potential of the dimer radical cation should be less negative by 0.65 and 0.59 V than that of the radical monomer radicals due to the stabilization energy. The $-\Delta G^0$ values for the reverse electron transfer from the dimer radical cation to $TPB^\bullet$ were thus estimated to be 1.04 and 1.02 eV for ($NS^+ \cdots NS^\bullet$) and ($DCS^+ \cdots DCS^\bullet$), respectively [39].

The observed values of $-\Delta G^0$ in this study for the reverse electron transfer of monomer radicals and dimer radical cations are in the Marcus inverted region [26,27]. The rate constant of the reverse electron transfer reactions from the dimer radical cation to $TPB^\bullet$ would become higher due to the smaller $-\Delta G^0$ in the inverted region. This is the reason why the observed decay was faster for dimer radical cations. These results strongly suggest the applicability of the present system to ultrafast optical switching in the NIR region if an appropriate combination of a donor anion and an acceptor cation is used.

4. Parallel all-optical processing in guided wave geometry containing organic dyes

4.1. Ultrafast spatial light modulation and parallel optical recording based on photoinduced complex refractive index changes upon nanosecond laser excitation

All-optical data processing has recently attracted much interest especially in the fields of spatial light modulation and optical data storage. A spatial light modulator (SLM) is a device to two-dimensionally control the intensity or the phase of reading light by another (writing) light, which plays an essential role in a projection TV, wavefront correction and an optical correlator. However, no practical devices have been developed except some prototypes or SLMs based on liquid crystals (LCs). The response time of LC-SLM is controlled by the electric field induced motion of LC; about a few hundreds of microseconds (μs) for ferroelectric LC and a few tens of milliseconds (ms) for nematic LC. The spatial resolution of LC-SLM is also not so high, about 10–20 μm, because a photoconducting layer used to optically address LC limits it. Recently multiple-quantum-well (MQW) SLMs have been developed showing spatial resolutions of 5–7 μm and a response time of 1 μs or faster [47–49]. MQW-SLMs will need further improvements in properties as spatial resolution, contrast, or capability of handling large readout intensities.

Several types of new devices for optical parallel data processing have been proposed based on surface plasmon resonance (SPR), guided wave mode and Fabry–Perot (FP) resonance [50–52]. However, all of these devices could not exceed the LC-SLM especially in the response time. Okamoto et al. [50] reported an all-optical photoaddressed SLM using a dye-doped polymer film in a surface plasmon resonance (SPR) configuration. They demonstrated the SLM based on photothermal changes in the refractive index of the methyl orange-doped poly(vinyl alcohol) (PVA) film using an Ar laser of 1–6 W cm^{-2} as a writing beam. The rise and fall times at 6 W cm^{-2} laser power were about 10 s and 2 s, respectively [50]. Yacoubian and Aye proposed Fabry–Perot (FP) resonance shifting in attenuated-total-reflection (ATR) geometry using azo-dye polymers [51]. They reported that their ATR-FP device enhanced optical modulation speed and efficiency as compared with the conventional intensity modulation based on photoinduced birefringence of Disperse Red 1 dye-doped poly(methylmethacrylate) [51]. The response time, 50–200 ms, was still relatively slow, though it was improved as compared with the conventional modulation system [51]. Ho et al. proposed a polarization vectorial holographic recording based on birefringent polymeric materials containing a photochromic azo benzene dye. The response time was 80 μs with a 100 mW power (80 $\mu J/cm^2$) of Ar laser [52]. Fichou et al. [53] proposed an incoherent-to-coherent optical converter based on photoinduced absorption of sexithiophene film. No actual properties of such a device, including the response time, were reported.

We have also proposed a novel all-optical SLM based on complex refractive index changes upon photoexcitation of an organic dye-doped polymer thin film [54–60]. Similar resonance shift in guided mode due to refractive index changes was first reported by Sekkat et al. [61,62] in photoisomerization of azobenzene derivatives in polymeric thin films by pumping at 546 nm. They studied photoisomerization and thermal relaxation by a shift of the reflectivity dips in the guided wave mode. The observed response time was 2–15 s, which was too slow to be used in spatial light modulation or optical memory [61,62]. The conformational changes (*trans* $\rightarrow$ *cis*) necessary in solid films and a smaller quantum yield of photoisomerization might contribute to such slow responses, though they did not show the value.

Our system is very unique as compared to the previously proposed "all-optical" light modulation systems as mentioned above. In principle fs response can be achieved in this system, because we use resonance condition changes of the guided optical waves (guided mode) in the ATR geometry based on the changes in the imaginary or the real part of the refractive index due to transient absorption or its Kramers–Kronig transformation, as schematically shown in Fig. 12. The guided mode "resonance" pattern depends not only on the thickness of the dielectric layer but also on its complex refractive index composed of real and imaginary parts, in general. If the imaginary part increases due to transient absorption, for example, the reflectance increases from curve **a** to **c** as shown in Fig. 12. A change of the real part shifts the resonance from curve **a** to **b** as shown in Fig. 12 for the case of a decrease. The intensity of the probe beam can be two-dimensionally controlled by the pump (writing) beam through photoexcitation of a dye. The main advantages using the guided mode are (1) its high sensitivity to small changes in refractive index and thickness, and (2) its sensitivity to both p- and s-polarized light. So far we have achieved repeated light modulation using a pulsed ns

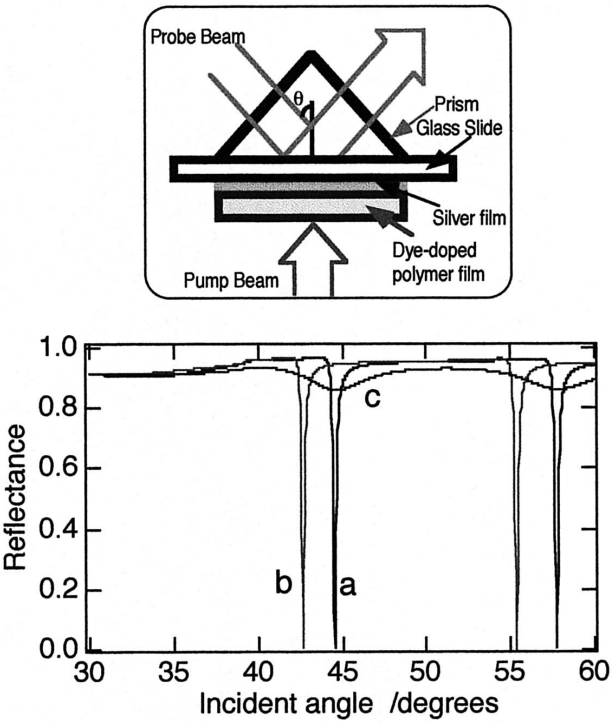

Fig. 12: Schematic representation of the all-optical parallel processing in guided mode geometry and the calculated reflectance for a polymer film (1600 nm) on a silver layer (50 nm). The complex refractive index of the polymer layer is (a) 1.60, (b) 1.58 and (c) $1.60 + 0.02i$.

laser and CuPcS and ZnPcS in guided wave-mode geometry. The response time was controlled by the triplet lifetime of phthalocyanines, 30 ns for CuPcS and 0.55 ms for ZnPcS. We are making efforts to achieve much faster responses using a ps or fs laser and appropriate materials.

We have also demonstrated self-held ultrafast parallel optical switching based on the same geometry and using photochromic compounds instead of phthalocyanines [55–58,60]. Absorption spectra of spiropyran derivative (SP) dispersed in polystyrene with a weight ratio of 1 : 10 are shown in Fig. 13 before and after UV irradiation for 5 s. Strong absorption in the visible region due to photomerocyanine (PM) can be held for a long time and be reverted to that of SP by visible irradiation. Spectra of extinction-coefficient and refractive-index changes (Δk and Δn) of polystyrene thin film containing SP upon UV excitation for 5 s are shown in Fig. 14. The former is based on the observed difference absorption spectra before and after UV irradiation as shown in Fig. 13. The latter is calculated from the extinction coefficient Δk by Kramers–Kronig transformation. Refractive-index changes with different signs can be seen near strong absorption changes. The extinction-coefficient and/or refractive-index changes over a wide wavelength range approximately from 400 to 800 nm can be utilized to operate a wide range all-optical switch. The guided mode structures are very important to

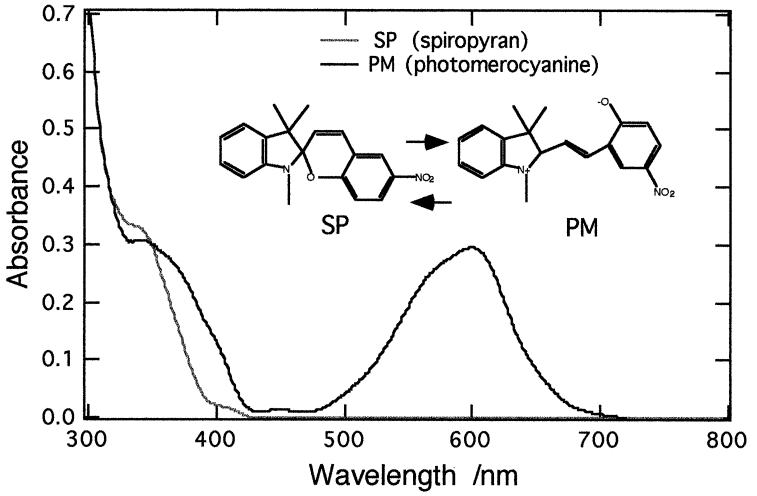

Fig. 13: The structures of photochromic SP and PM, and absorption spectra of SP or PM dispersed in a polystyrene thin film with a weight ratio of 1 : 10 before and after UV irradiation.

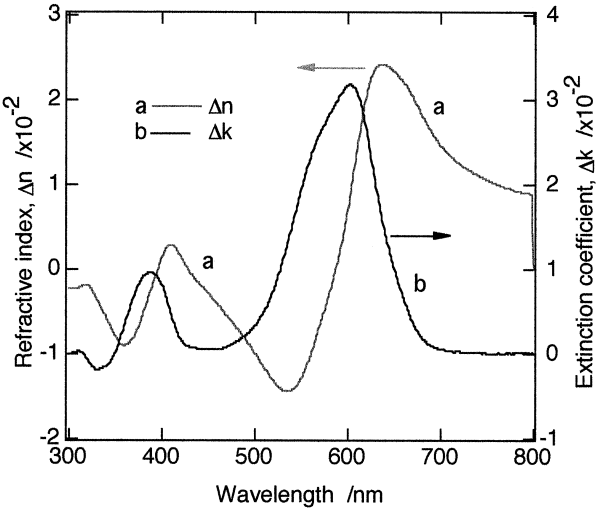

Fig. 14: Spectra of (a) extinction coefficient and (b) refractive index of polystyrene thin film containing SP and PM. The former is based on the observed difference absorption spectra shown in Fig. 13 before and after UV irradiation. The latter was calculated from (a) by Kramers–Kronig transformation.

utilize ultrafast changes of molecular electronic state upon photoexcitation for practical photonics devices.

The incident-angle dependences of measured reflectance of a probe beam at 543 nm are shown in Fig. 15 for a polystyrene film containing SP with a weight ratio of 10 : 1. Each dip shows the SPR for a silver film (**a**) and the guided TM wave mode for the composite thin film before (**b**) and after (**c**, **d**) excitation by a pulsed Nd–YAG laser

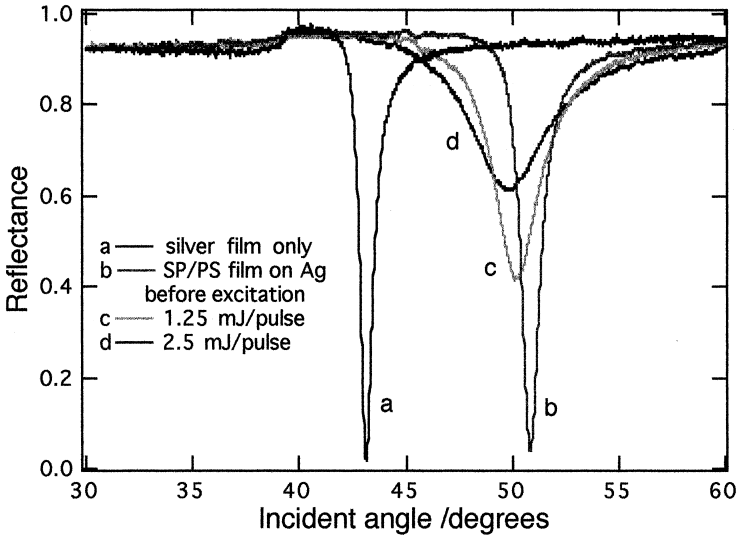

Fig. 15: Incident-angle dependences of observed reflectance of a glass slide covered with (a) a silver film (50 nm) alone, and an SP in polystyrene (1 : 10) film (264 nm thick), (b) before, and (c), (d) after ns laser excitation (1.25 and 2.5 mJ/pulse, respectively) at 355 nm.

at 355 nm. The power of the pulsed laser at 355 nm was set to 1.25 or 2.5 mJ/pulse. Photochromism induced by transformation from SP to PM increased the reflectance and slightly shifted the dip to lower incident angles from curve **b** to **c** or **d** as shown in Fig. 15. The simulation gave almost perfect reproduction of the observed results, from which the complex refractive indices before and after excitation were determined. From comparison between the measured and calculated dependences, the thickness of the silver film and the polymer film was evaluated as 50 nm and 264 nm, respectively. The reflectance at the incident angle of 50.76° was increased from 0.04 to 0.68 upon excitation as shown in Fig. 15. The reflectance increase and the shift were found to be due to the increase of extinction coefficient and the decrease of refractive index at 543.5 nm of the polystyrene thin film containing SP as shown in Fig. 13 by the formation of the PM form. The changes of refractive index and extinction coefficient were estimated to be −0.015 and +0.024 at 2.5 mJ/pulse from comparison between the measured and the calculated dependences. Transmittances of the probe beam before and after excitation at 2.5 mJ/pulse were calculated as comparison to the present reflectance changes by using the same value for the film thickness and the extinction coefficient changes. The estimated values were 0.99 and 0.86 at 543 nm before and after excitation, respectively. The dynamic range of reflection changes, 17.0, was thus demonstrated to be much better than that of transmission changes, 1.15.

The reflectance at the incident angle of 50.76° increased by 5–10 times very rapidly with a rise time of about 20 ns upon pulsed laser excitation at 355 nm, depending on its power. This rise time corresponded to the response of a photomultiplier. Much better switching is expected if a picosecond laser and an experimental setup with much better

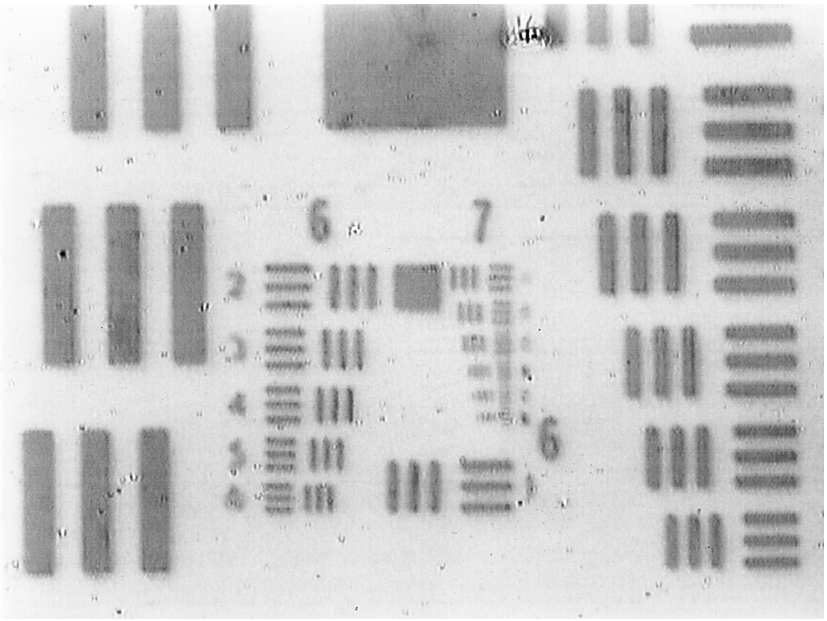

Fig. 16: Image (×500) written through a USAF Test Target as a mask by a single shot of ns 355 nm laser (1 mJ/pulse) on a spiropyran-doped poly(styrene) film deposited on a silver film.

time resolution are used, since the rise time of transient absorption of a polystyrene film containing spiropyran was reported as about 200 ps upon excitation with a ps laser [63]. The reflectance after ns pulsed laser excitation at 355 nm was held at a high value without applied power. The switching OFF was also demonstrated to be very fast with a response time similar to that of switching ON, although its accurate estimation was difficult due to a smaller S/N ratio. These results indicate that this fast reflectance decrease was caused by the reverse photochromic reaction from PM to SP, and not by the thermal reaction. The observed smaller reflectance change as compared with switching ON was due to a lower quantum yield of ring closure of PM. Photochromic dyes which have a higher quantum yield for reverse photochromic reaction will switch from ON to OFF with a larger dynamic range and fast response.

Wavelength dependences of the refractive index and the extinction coefficient changes evaluated from reflectance changes upon pulsed laser excitation in the polystyrene film containing SP corresponded well with the spectra of extinction-coefficient and refractive-index changes estimated from steady photolysis as shown in Fig. 14. These results confirmed the mechanism responsible for the reflectance changes in guided wave geometry and also demonstrated the wide range of operation wavelength of the present all-optical device.

In addition to very fast photoresponses, it is essential to write and read a two-dimensional image pattern for optical parallel data processing. Fig. 16 shows microscopic photographs (×500) of the image written through a USAF Test Target as a mask by a single shot of ns 355 nm laser (1 mJ/pulse) on a spiropyran-doped PS film

deposited on a silver film. At least 128 line pairs/mm was clearly seen, which corresponds to a spatial resolution of 3.9 μm. Hickel et al. reported that the lateral resolution of optical waveguide microscopy based on the resonance shift by using guided waves as illumination light source is better than 10 μm [64]. The spatial resolution in these imaging devices based on guided mode geometry is limited by the propagation length of the guided waves, which is reduced by coupling to surface plasmon states in the case of p-polarized light.

As one of the applications of the present all-optical switch in the near future, the architectures of the optical parallel processing logic devices AND and OR were proposed [58]. Optical parallel AND and OR devices are composed of two present switches and one switch only, respectively. They are operated by two parallel data as two input signals, Input 1 and Input 2. An optical parallel NOT device will also be composed by a polymer film containing a photochromic dye which will be colored only during irradiation. Then, the excitation light as input signal causes an intensity decrease of a probe beam as output signal. A combination of the present all-optical switch and the photon-mode spatial light modulator will also contribute a great deal to construct an ultrafast parallel processing optical correlator. Several spatial optical logic devices can be composed simply and easily from the present all-optical switch which employs reflectance increase or decrease by irradiation. An example of possible all-optical parallel correlation based on the present device is schematically shown in Fig. 17.

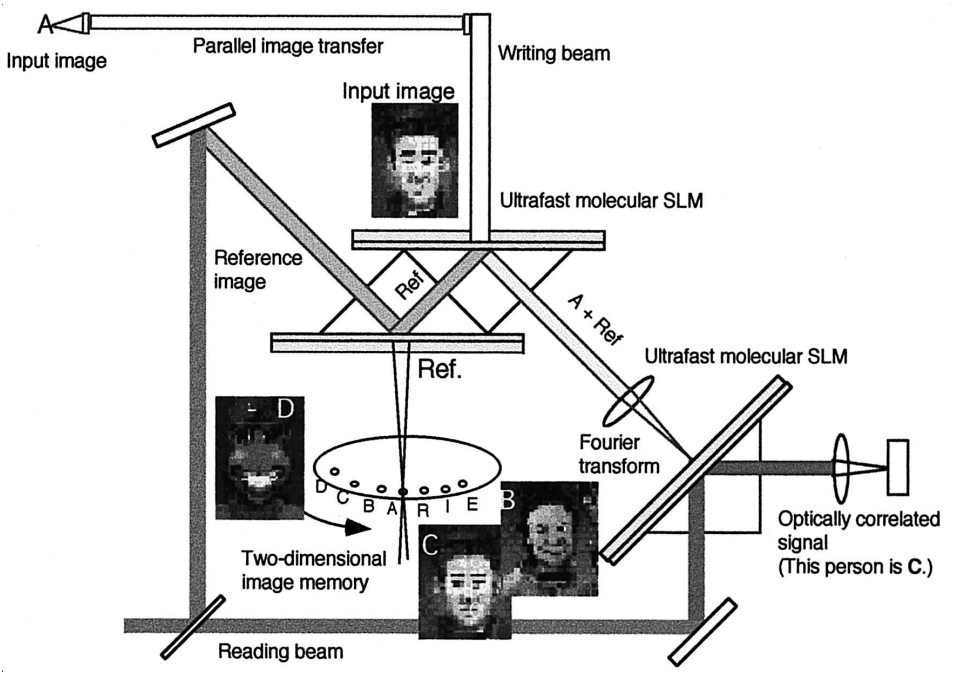

Fig. 17: Schematic representation of a possible all-optical parallel correlation system based on the present device.

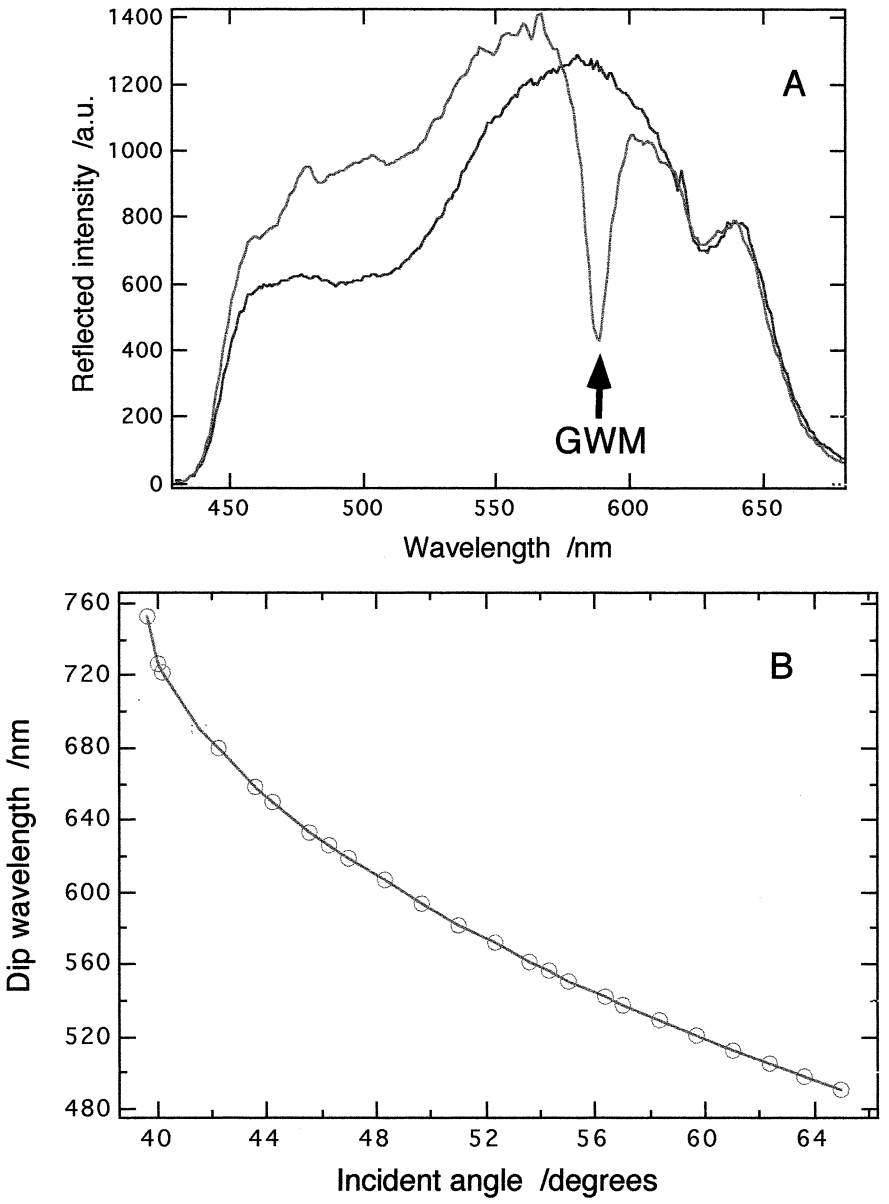

Fig. 18: (A) Profiles of fs white light without and with a spin-coated Arton® film at an incident angle of 50.0°. (B) Relationship between the dip wavelength and incident angle for a spin-coated 360 nm thick film of spiropyran/Arton® (1 : 2) observed with fs white light.

4.2. Reversible reflectance control of fs white light in guided wave geometry containing photochromic compounds upon fs laser photoexcitation

As mentioned in the previous section, our all-optical SLM or optical switching device based on complex refractive index changes upon photoexcitation of an organic dye-doped polymer thin film can make in principle fs response, because we use resonance condition changes of the guided optical waves (guided mode) in the ATR geometry based on photoinduced changes of the imaginary or the real part of the refractive index. In order to demonstrate it, we employed photochromic spiropyran in a fs pump-probe measurement system as shown in Fig. 4. Profiles of detected fs white light are shown in Fig. 18(A) at an incident angle $\theta = 50.0°$ without and with a 360 nm thick Arton® film containing SP. The dip found around 588 nm in Fig. 18(A) is due to the guided wave mode. The dip wavelength shifted to the longer side by decreasing the incident angle, as shown in Fig. 18(B), from about 500 nm at $\theta = 65°$ to about 760 nm at $\theta = 39°$. This film showed highly efficient photochromism upon fs laser excitation at 400 nm, as shown in Fig. 19. Changes of reflected light intensity for SP/Arton® (1 : 2) film (360 nm) at $\theta = 53.0$, 50.0, 42.6, and 39.6° upon fs laser excitation at 400 nm and He–Ne laser at 543.5 nm are shown in Figs. 20–23, respectively. All reflectance changes were highly reversible, corresponding to photochromism between SP and PM forms. The "direction" of changes of reflectance clearly depended on the incident angle or the dip wavelength. By photochromism from SP to PM, the reflectance increased with shifting the dip wavelength to the shorter side at $\theta = 53.0°$ and to the longer side at $\theta = 42.6°$, or at almost the same wavelength at $\theta = 50.0°$. At an incident angle of $\theta = 39.6°$, the dip wavelength shifted to the longer side with almost no changes of reflectance. Upon CW He–Ne laser irradiation at 543.5 nm, all dips returned to the original position before

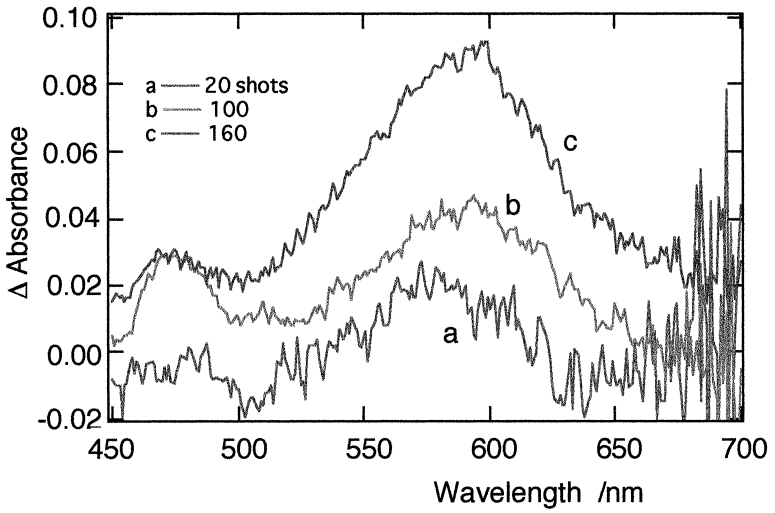

Fig. 19: Absorption spectra of SP/Arton® (1 : 2) film (360 nm thick) upon fs laser excitation at 400 nm with 20–160 shots.

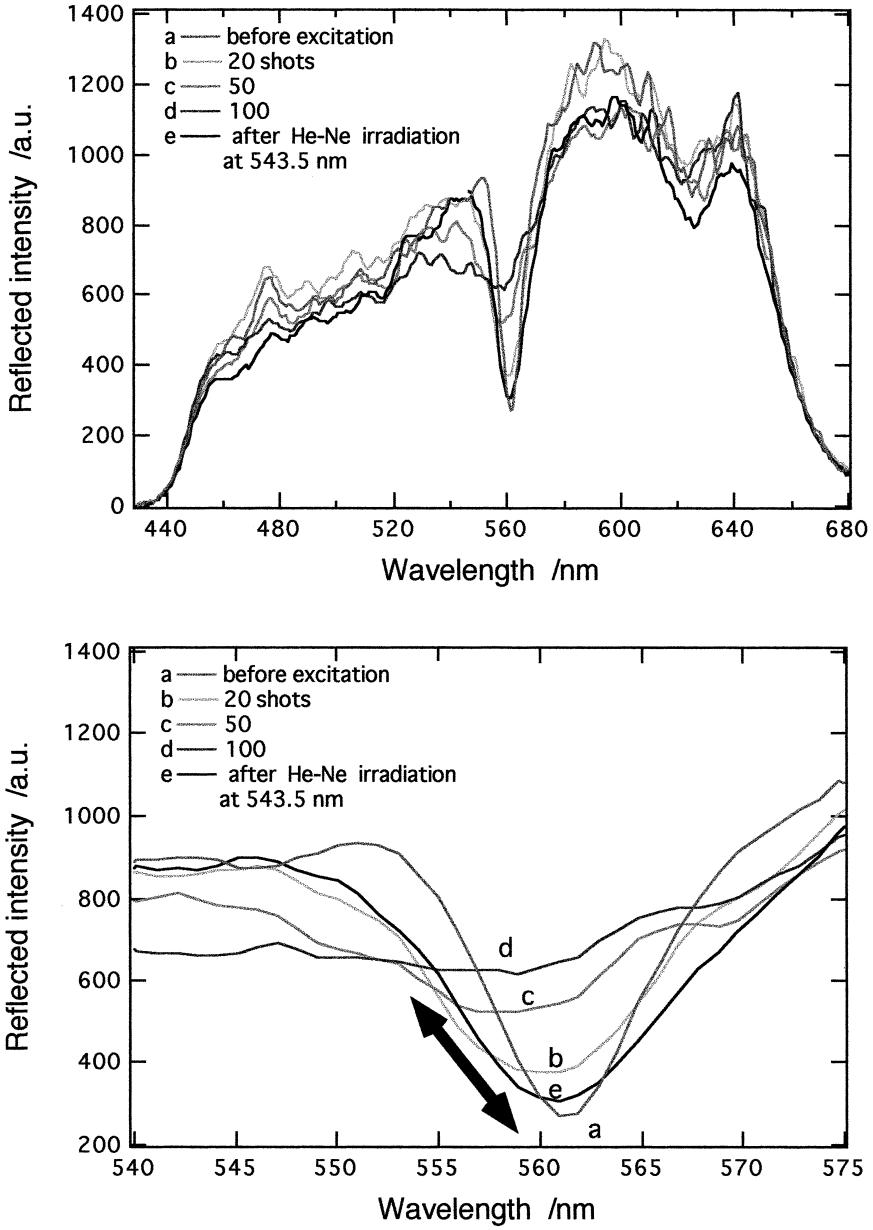

Fig. 20: Changes of reflected light intensity for SP/Arton® (1 : 2) film (360 nm thick) at an incident angle of 53.0° upon fs laser excitation at 400 nm and He–Ne laser at 543.5 nm.

fs laser excitation due to reverse photochromism from PM to SP. These results clearly indicate that fs white light can be used as a probe light in guided mode geometry and that the fs pump-probe method will be used in such geometry. Efforts are being

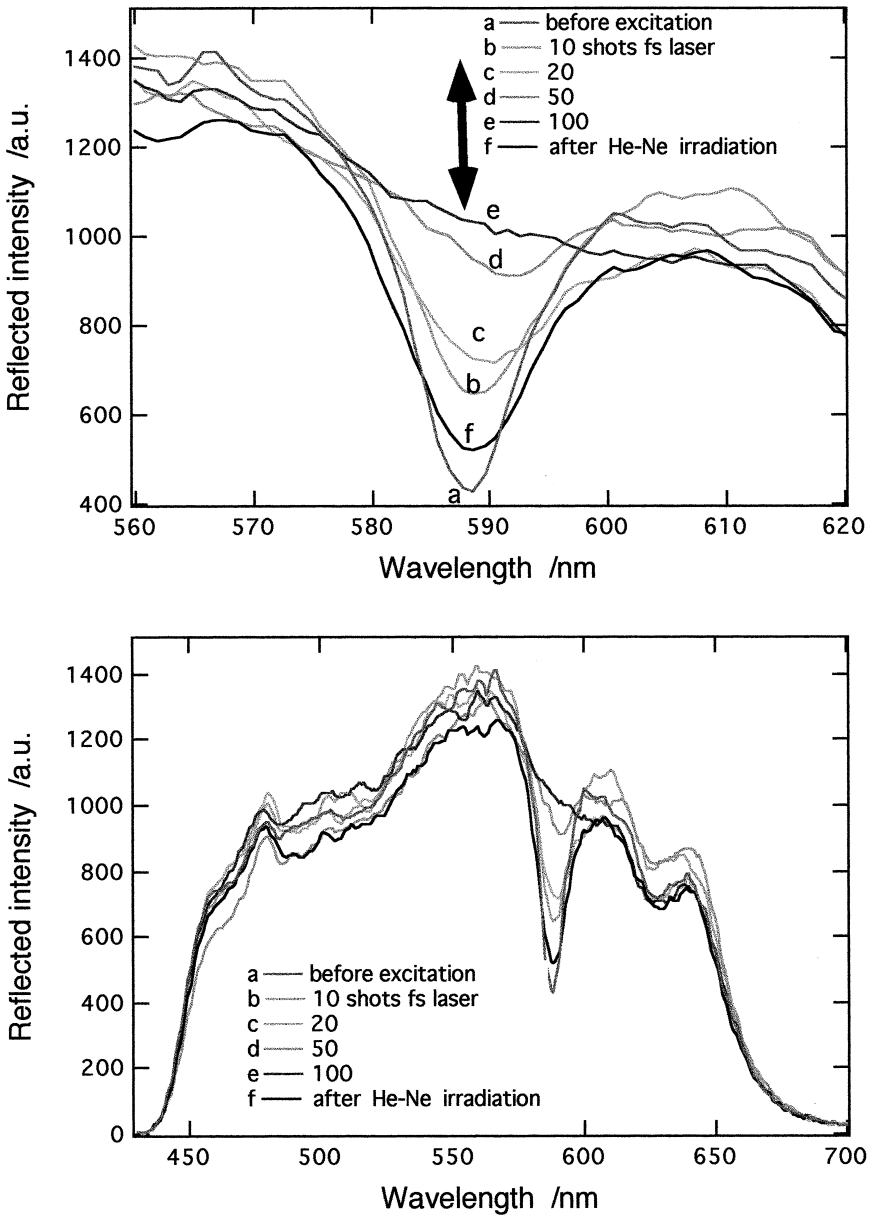

Fig. 21: Changes of reflected light intensity for SP/Arton® (1 : 2) film (360 nm) at an incident angle of 50.0° upon fs laser excitation at 400 nm and He–Ne laser at 543.5 nm.

made to construct fs SLM based on the guided mode geometry and appropriate ultrafast photoresponsive materials.

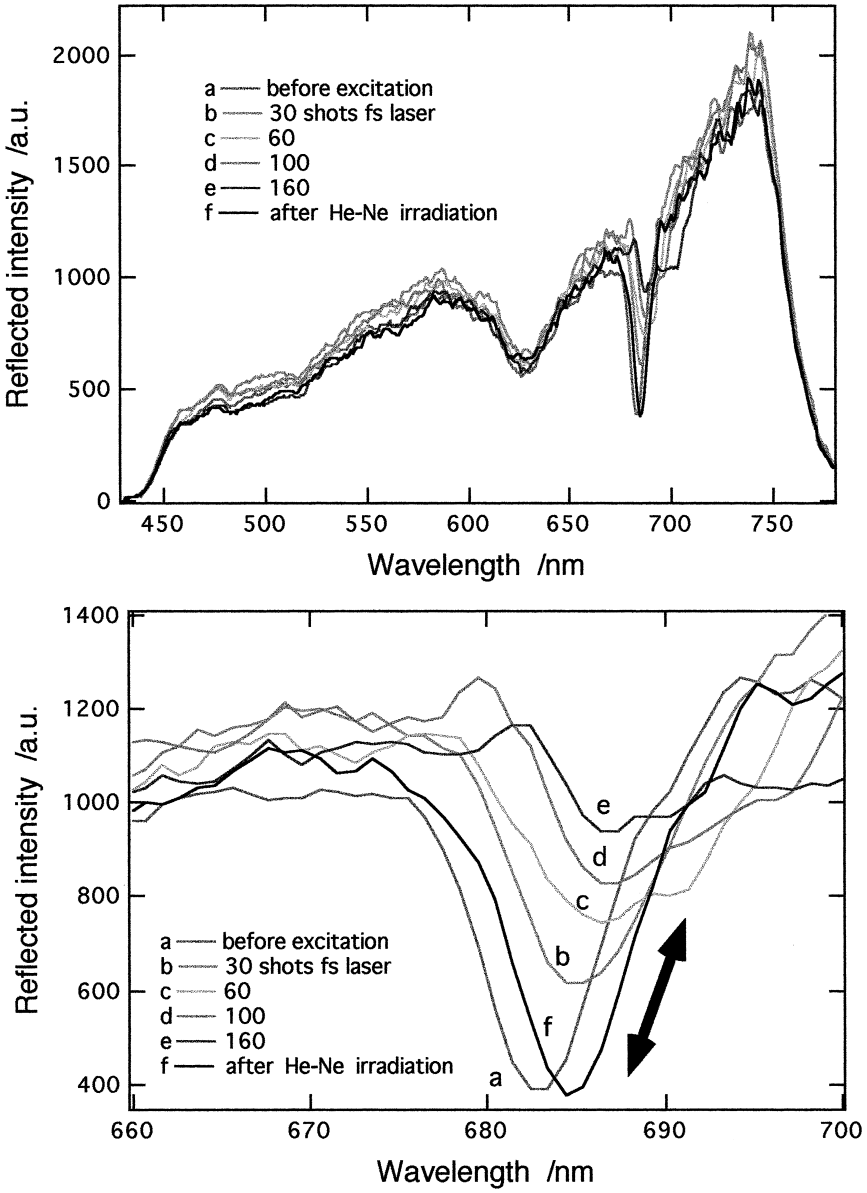

Fig. 22: Changes of reflected light intensity for SP/Arton® (1 : 2) film (360 nm) at an incident angle of 42.6° upon fs laser excitation at 400 nm and He–Ne laser at 543.5 nm.

5. Ultrafast nonlinear optical responses amplified by photoexcitation

Nonlinear optical responses are very important to achieve, for example, wavelength conversion, electro-optical or pure optical control of the refractive index, and all-optical

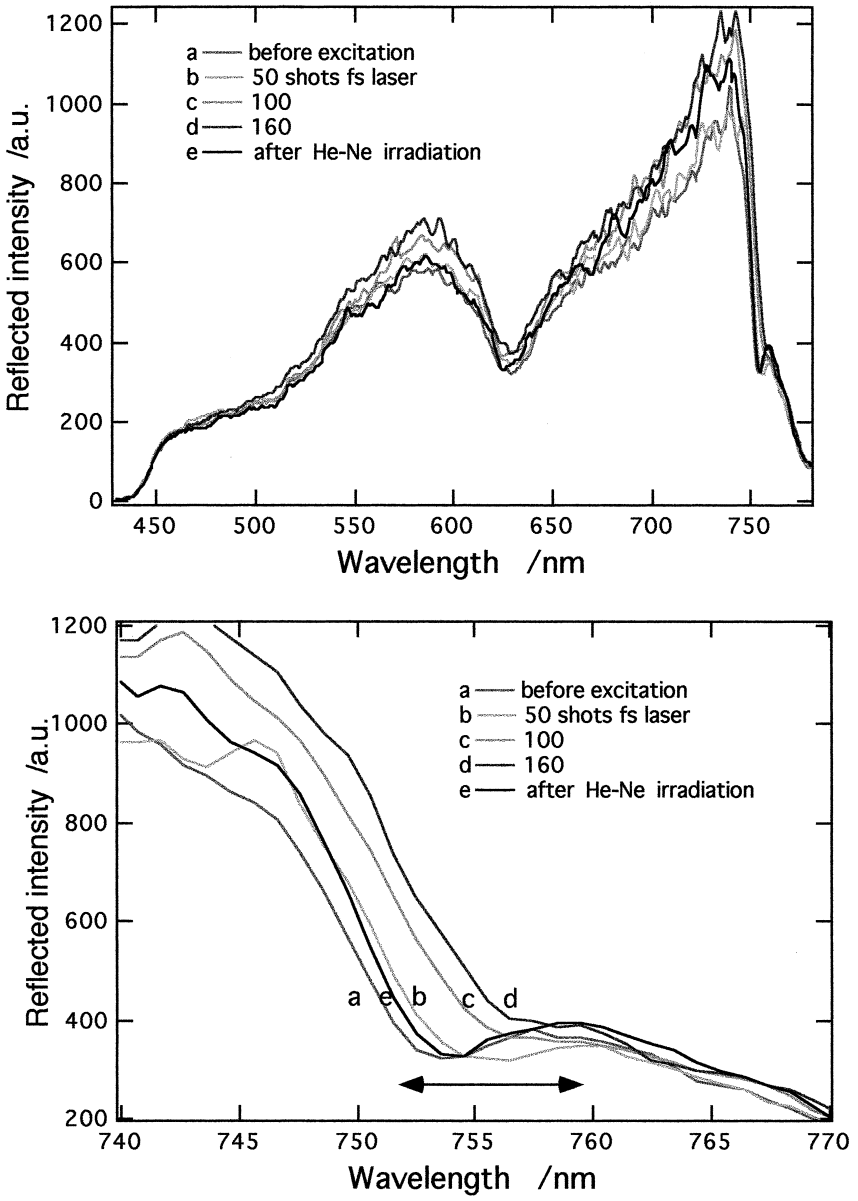

Fig. 23: Changes of reflected light intensity for SP/Arton® (1 : 2) film (360 nm) at an incident angle of 39.6° upon fs laser excitation at 400 nm and He–Ne laser at 543.5 nm.

logic. Many organic and inorganic materials have been developed. One of the main problems especially in organic compounds is the small nonlinear optical coefficient. We have also been making efforts to modulate or enhance the second- and the third-order nonlinear optical properties by changing the electronic state or the extent of electronic

distribution upon photoexcitation [65–73]. We also observed considerable enhancement of the second- and the third-order optical nonlinearity upon photoexcitation [68–73].

6. Conclusion

We have developed several molecules and organized molecular assemblies to control the lifetime of the colored state by photoinduced electrochromism, the complex refractive index, and the nonlinear optical responses by the interactions with photons. Application of such materials to novel optical devices based on photoinduced complex refractive index changes was proposed and was successfully demonstrated in photon-mode recording and reflection control. These results will contribute a great deal to realize parallel all-optical ultrafast data processing devices. Considering that our vision is initiated by a simple photoisomerization of 11-*cis* retinal and is processed in a parallel way to achieve extreme high functions, molecular photonics based on elegant combination of molecules, photons and appropriate devices is expected to be the very promising way of ultrafast information processing in the near future.

Acknowledgements

The author would like to thank Dr. K. Sakai, Dr. H. Sakaguchi, Dr. H. Kawai, Dr. K. Sasaki, Dr. D. Matsunaga, Mr. S. Kashihara, Dr. S.H. Park, Mr. T. Adachi, and Mr. I. Yoshida for their great contributions. Partial supports by the Grant-in-Aids for Scientific Research on Priority Areas "Molecular Superstructures, Design and Creation" (No. 07241102), Monbusho International Scientific Research Program (Joint Research, No. 08044137, 10044144), "Creation of Novel Delocalized Electronic Systems", (No. 10146219), and "Molecular Synchronization for Design of New Materials System" (No. 11167242, 13022230), from the Ministry of Education, Science, Sports and Culture, Japan are greatly acknowledged.

References

1. T. Kamiya, F. Saito, O. Wada, and H. Yajima (Eds.), *Femtosecond Technology*, Springer Series in Photonics 2, Series Eds. T. Kamiya, B. Monemar, and H. Venghaus (Springer-Verlag, Berlin, 1999).
2. T. Nagamura, Ch. VI-4 in Ref. [1], (1999), p. 376.
3. T. Nagamura, in *Sensors and Optical Switching*, Molecular and Supramolecular Photochemistry Series, Vol. 7, edited by V. Ramamurthy and K. S. Schanze (Marcel Dekker, New York, 2001) p. 387.
4. H. Dürr and H. Bouas-Laurent, *Photochromism Molecules and Systems* (Elsevier, Amsterdam, 1990).
5. M. Irie, Chem. Rev. **100** (5), 1685 (2000) and references cited therein.
6. Y. Yokoyama, Chem. Rev. **100** (5), 1717 (2000) and references cited therein.
7. G. Berkovic, V. Krongauz, and V. Weiss, Chem. Rev. **100** (5), 1741 (2000) and references cited therein.
8. T. Nagamura and K. Sakai, J. Chem. Soc. Faraday Trans. 1 **84**, 3529 (1988).
9. T. Nagamura and S. Muta, J. Photopolym. Sci. Technol. **4**, 55 (1991).
10. T. Nagamura and K. Sakai, J. Chem. Soc. Chem. Commun., 810 (1986) .

11. T. Nagamura and K. Sakai, Ber. Bunsenges. Phys. Chem. **93**, 1432 (1989).
12. T. Nagamura, K. Sakai, and T. Ogawa, J. Chem. Soc. Chem. Commun., 1035 (1988).
13. T. Nagamura and K. Sakai, Thin Solid Films **179**, 375 (1989).
14. T. Nagamura and Y. Isoda, J. Chem. Soc. Chem. Commun., 72 (1991).
15. T. Nagamura, Polym. Int. **27**, 125 (1992).
16. T. Nagamura, S. Muta, and K. Sakai, J. Photopolym. Sci. Technol. **5**, 561 (1992).
17. T. Nagamura, Mol. Cryst. Liq. Cryst. **224**, 75 (1993).
18. T. Nagamura, H. Sakaguchi, S. Muta, and T. Ito, Appl. Phys. Lett. **63**, 2762 (1993).
19. T. Nagamura, H. Sakaguchi, T. Ito, and S. Muta, Mol. Cryst. Liq. Cryst. **247**, 39 (1994).
20. T. Nagamura, H. Sakaguichi, and S. Muta, Proc. SPIE **2514**, 241 (1995).
21. T. Nagamura, Pure Appl. Chem. **68** (7), 1449 (1996).
22. H. Inoue, H. Sakaguchi, and T. Nagamura, Appl. Phys. Lett. **73**, 10 (1998).
23. T. Nagamura and K. Sakai, Chem. Phys. Lett. **141**, 553 (1987).
24. T. Nagamura and K. Sakai, Ber. Bunsenges. Phys. Chem. **92**, 707 (1988).
25. H. Nishida, N. Takada, M. Yoshimura, T. Sonoda, and H. Kobayashi, Bull. Chem. Soc. Jpn. **57**, 2600 (1984).
26. R.A. Marcus, J. Chem. Phys. **24**, 966 (1956).
27. J.R. Miller, L.T. Calcaterra, and G.L. Closs, J. Am. Chem. Soc. **106**, 3047 (1984).
28. T. Nagamura, H. Sakaguchi, K. Suzuki, C. Mochizuki, and K. Sasaki, J. Photopolym. Sci. Technol. **6**, 133 (1993).
29. T. Nagamura, H. Sakaguchi, K. Sasaki, C. Mochizuki, and K. Suzuki, Thin Solid Films **243**, 660 (1994).
30. T. Nagamura, D. Kuroyanagi, K. Sasaki, and H. Sakaguchi, Proc. SPIE **2547**, 320 (1995).
31. K. Sasaki and T. Nagamura, J. Photopolym. Sci. Technol. **9**, 129 (1996).
32. K. Sasaki and T. Nagamura, Mol. Cryst. Liq. Cryst. **294**, 145 (1997).
33. H. Kawai, K. Nakano, and T. Nagamura, Chem. Lett., 1300 (2001).
34. T. Nagamura, A. Tanaka, H. Kawai, and H. Sakaguchi, J. Chem. Soc. Chem. Commun., 599 (1993).
35. T. Nagamura, H. Kawai, T. Ichihara, and H. Sakaguchi, Synth. Metals **71**, 2069 (1995).
36. H. Kawai and T. Nagamura, Mol. Cryst. Liq. Cryst. **267**, 235 (1995).
37. T. Nagamura, T. Ichihara, and H. Kawai, J. Phys. Chem. **100**, 9370 (1996).
38. T. Nagamura, S. Kashihara, and H. Kawai, Chem. Phys. Lett. **294**, 167 (1998).
39. H. Kawai and T. Nagamura, J. Chem. Soc. Faraday Trans. **94**, 3581 (1998).
40. W.-S. Xia, H. Kawai, and T. Nagamura, J. Photochem. Photobiol. A: Chem. **136** (1–2), 35 (2000).
41. H. Kawai and T. Nagamura, Mol. Cryst. Liq. Cryst. **344**, 209 (2000).
42. S.H. Park, H. Kawai, and T. Nagamura, J. Photopolym. Sci. Technol. **13** (2), 197 (2000).
43. S.H. Park and T. Nagamura, Mol. Cryst. Liq. Cryst. **370**, 249 (2001).
44. S.H. Park and T. Nagamura, J. Photopolym. Sci. Technol. **14** (2), 227 (2001).
45. S.H. Park and T. Nagamura, J. Chem. Soc. Chem. Commun., 2344 (2001).
46. S.H. Park, H. Kawai, and T. Nagamura, J. Chem. Soc. Perkin Trans. 2 (3), 508 (2002).
47. A. Partori, A.M. Glass, T.H. Chiu, and D.T.H. Liu, Opt. Lett. **18**, 906 (1993).
48. P. Tayebati, E. Canoglu, C. Hantzis, and R.N. Sacks, Appl. Phys. Lett. **71**, 1610 (1997).
49. S.R. Bowman, W.S. Rabinovich, G. Beadie, S.M. Kirkpatrick, D.S. Katzer, K. Ikossi-Anastasiou, and C.L. Adler, J. Opt. Soc. Am. B **15**, 640 (1998).
50. T. Okamoto, T. Kamiyama, and I. Yamaguchi, Opt. Lett. **18**, 1570 (1993).
51. A. Yacoubian and T.M. Aye, Appl. Opt. **32**, 3073 (1993).
52. Z.Z. Ho, G. Savant, J. Hirsh, and T. Jannson, Proc. SPIE **1773**, 433 (1992).
53. D. Fichou, J.-M. Nunzi, F. Charra, and N. Pfeffer, Adv. Mater. **6**, 64 (1994).
54. T. Nagamura and T. Hamada, Appl. Phys. Lett. **69**, 1191 (1996).
55. K. Sasaki and T. Nagamura, Appl. Phys. Lett. **71**, 434 (1997).
56. K. Sasaki and T. Nagamura, J. Appl. Phys. **83**, 2894 (1998).
57. T. Nagamura and K. Sasaki, Proc. SPIE **3466**, 212 (1998).
58. T. Nagamura and K. Sasaki, Mol. Cryst. Liq. Cryst. **344**, 199 (2000). .
59. T. Nagamura, T. Adachi, I. Yoshida, H. Inoue, H. Heckmann, and M. Hanack, Mol. Cryst. Liq. Cryst. **370**, 97 (2001).

60. T. Nagamura, K. Sasaki, F. Iizuka, T. Adachi, and I. Yoshida, Opt. Commun. **205**, 107 (2002).
61. Z. Sekkat and M. Dumont, Appl. Phys. B **53**, 121 (1991).
62. Z. Sekkat, D. Morichere, M. Dumont, R. Loucif-Saibi, and J.A. Delaire, J. Appl. Phys. **71**, 1543 (1992).
63. T. Ito, M. Hiramatsu, M. Hosoda, and Y. Tsuchiya, Rev. Sci. Instrum. **62**, 1415 (1991).
64. W. Hickel and W. Knoll, Appl. Phys. Lett. **57**, 1286 (1990).
65. H. Sakaguchi, T. Nagamura, and T. Matsuo, Jpn. J. Appl. Phys. **30**, L377 (1991).
66. T. Nagamura, H. Sakaguchi, and T. Matsuo, Thin Solid Films **210**/**211**, 160 (1992).
67. H. Sakaguchi, L.A. Gomez-Jahn, M. Prichard, T.L. Penner, D.G. Whitten, and T. Nagamura, J. Phys. Chem. **97**, 1474 (1993).
68. H. Sakaguchi and T. Nagamura, Nonlinear Optics **15**, 73 (1996).
69. H. Sakaguchi and T. Nagamura, in *Ultrafast Phenomena X*, edited by P.F. Barbara, J.G. Fujimoto, W.H. Knox and W. Zinth (Springer-Verlag, Berlin, 1996) pp. 62, 209.
70. A. Harada and T. Nagamura, Mol. Cryst. Liq. Cryst. **316**, 79 (1998).
71. A. Harada and T. Nagamura, Nonlinear Optics **22**, 169 (1999).
72. H. Sakaguchi and T. Nagamura, Nonlinear Optics **22**, 413 (1999).
73. T. Nagamura, T. Umeda, and H. Sakaguchi, Mol. Cryst. Liq. Cryst. **370**, 119 (2001).